Aqueous Graphene Dispersions—Optical Properties and Stimuli-Responsive Phase Transfer

David Ager,[†] Vivek Arjunan Vasantha,[†,§] Rene Crombez,[†] and John Texter*[,†,‡]

[†]Coating Research Institute and School of Engineering Technology, College of Technology, Eastern Michigan University, Ypsilanti, Michigan 48197, United States, and [‡]Department of Polymer Science and Engineering, College of Chemistry, Chemical Engineering and Materials Science, Soochow University, Suzhou 215123, China. [§]Present address: Institute of Chemical and Engineering Sciences (ICES), Agency for Science, Technology and Research (A*STAR), 1 Pesek Road, Jurong Island, Singapore 627833.

ABSTRACT We demonstrate essentially complete exfoliation of graphene aggregates in water at concentrations up to 5% by weight (166-fold greater than previous high concentration report) using recently developed triblock copolymers and copolymeric nanolatexes based on a reactive ionic liquid acrylate surfactant. We demonstrate that the visible absorption coefficient in aqueous dispersion, 48.9 ± 1.3 cm^2/mg at 500 nm, is about twice that currently accepted, and we show that this value is a greatest lower bound to extant macroscopic single sheet optical studies of graphene when one considers both fine structure constant and excitonic mechanisms of visible absorption. We also show that dilute and concentrated graphene dispersions are rheo-optical fluids that exhibit an isotropic to nematic transition upon application of a shear field, and we demonstrate stimuli-responsive phase transfer.

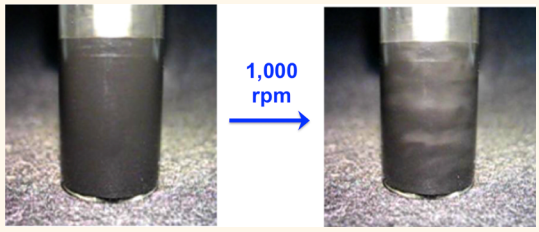

KEYWORDS: graphene · aqueous graphene dispersion · graphene absorption coefficient · rheo-optical fluid

The dispersion of graphene in various solvents provides motivation to make graphene more industrially processable, enabling bulk transport by pumping and accurate volumetric metering and by making graphene coatable on microscopic to macroscopic length scales.[1−6] Such dispersion processing also mitigates against possible untoward inhalation effects (post dry graphene processing).[7−9] A focus on dispersing graphene in water has arisen because of environmental concerns about limiting volatile organic emissions into the atmosphere and minimizing toxic exposure effects. Since stable colloidal dispersions require "particle" dimensions of the order of microns and smaller, graphene dispersions at present are not targeted for applications that require large area single or few layer sheets, such as needed in displays with areas greater than 25 cm^2.[4,10] This exclusion may change as our ability to thermally and chemically anneal and dope[11] graphene coatings becomes more sophisticated. Graphene dispersions are expected to provide electrically conducting inks particularly suited for flexible electronics[12−14] and highly thermally conducting coatings.[15−17] They are also being studied for many nanocomposite applications.[18−28] The cost of graphene is much less than that of other nanoscale carbons such as single wall or multiwall carbon nanotubes (SWCNT and MWCNT, respectively) and fullerenes, while graphene's electron and phonon transport properties are competitive with those of nanotubes.[29−33]

Investigations of dispersing graphene in water basically have followed similar efforts to disperse SWCNT[34−40] and MWCNT[41−47] in water using various surfactants and polymers as stabilizers. Stabilized aqueous graphene dispersions can be distinguished from nonaqueous dispersions[48−55] and from the competitive approach of creating oxidized graphene oxide (GO) from graphite, dispersing this GO in water or other solvent, and then chemically reducing this GO to reduced graphene oxide, rGO.[56−61] Each approach has some favored applications. Our goal in this paper is to demonstrate the high potential for making scalable aqueous graphene dispersions at concentrations that are truly

* Tel: 1-734-487-4587. E-mail: jtexter@emich.edu.

Received for review May 30, 2014 and accepted October 22, 2014.

Published online October 22, 2014
10.1021/nn502946f

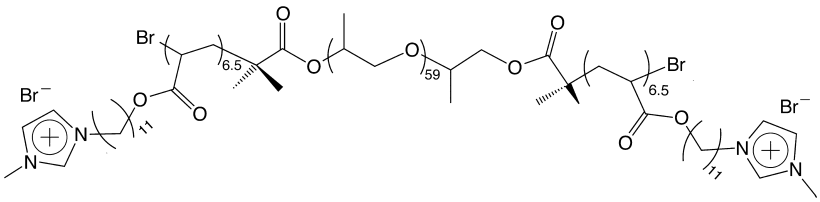

Scheme 1. TB Triblock Structure

practical and that will facilitate and support kilogram and higher volume manufacturing processes when needed. Another of our goals is to provide an unequivocal characterization of the optical properties of graphene in dispersion in the visible region. Light absorption is a key parameter needed for the rational design and evaluation of many devices and materials.[62,63]

Quite a few experimental studies have observed that the optical absorption in the visible apparently increases as more sonication is applied in dispersions of various concentrations as well as in various solvents.[51,64−68] This phenomenon has also been seen repeatedly in studies of dispersing carbon nanotubes.[69−72] It is then empirically established that the optical absorption of graphene becomes more pronounced as exfoliation proceeds, and it would seem logical that this absorption would become a maximum when few layer platelets become completely exfoliated into single sheets. The interaction of adjacent sheets in contact with one another serves, apparently, to dampen the visible absorption. If this effect derives from selection rules, it will be useful to transform some of the high-quality theoretical treatments into more localized molecular treatments understandable in terms of electronic dipole transition moments. However, a significant gap has persisted to this point between the optical absorption measurements performed on graphene dispersions and theoretical and experimental optical studies of pristine graphene under various conditions. An unequivocal connection between these limits will be made in discussions of our results.

The previously reported highest concentration dispersion of exfoliated graphene in water was 0.3 mg/mL.[64] In that report from Coleman and co-workers, it was noted that achieving 1 mg/mL by aqueous surfactant-stabilized exfoliation "would be a significant achievement."[64] In this paper, we examine the aqueous dispersion performance (stabilization during exfoliation) of two stabilizers: a triblock copolymer and a nanolatex (NL) that are based upon an ionic liquid monomer. These stabilizers may be termed polymerized ionic liquids (PIL).[73−77] Our graphene samples were obtained as aggregated powders composed of platelets of nominally 4.5−10 μm lateral dimension and about 35 graphene sheets thick. The crude dispersions were formulated at 1% to 4% graphene by weight,

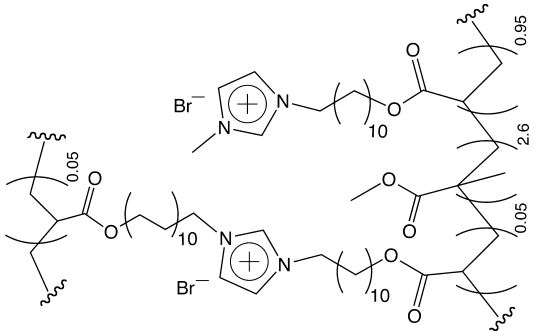

Scheme 2. Nanolatex Copolymer Structure

and we demonstrate essentially complete exfoliation without having to centrifuge to eliminate poorly dispersed components. We obtain very good uniformity in our visible optical characterizations of these dispersions, and we then show that these results are consistent with optical characterizations of macroscopic graphene sheets. We then demonstrate that these concentrated and dilute dispersions are rheo-optical fluids and that shear can be used to align these graphene sheets in suspension to produce constructive reflectance. A stimuli responsiveness associated with the stabilizers is used to demonstrate phase transfer of our dispersions, allowing dispersions prepared in one solvent to be easily reformed in another solvent.

Our stabilizers are based upon the ionic liquid acrylate surfactant, 1-(11-acryloyloxyundecyl)-3-methylimidazolium bromide (ILBr).[78,79] This monomer has been used to develop several stimuli-responsive materials, wherein the stimuli responsiveness emanates from the solubility variations exhibited by imidazolium anion ion-pairs when undergoing anion exchange or solvent exchange.[80,81] In previous work on dispersing SWCNT, MWCNT, and hydrothermal carbon in water, we found that the monomer ILBr as itself (as a surfactant), in a homopolymer, in linear copolymers, in triblock copolymers, and in nanolatexes provides active stabilization of graphenic surfaces by adsorbing onto such surfaces through $\pi-\pi$ overlap and by providing a water-loving functional group, hygroscopic imidazolium bromide.[82−86]

We investigated the efficacy of a triblock copolymer TB (Scheme 1) and a nanolatex copolymer (Scheme 2) of ILBr and methyl methacrylate (MMA). This triblock had a molecular weight M_n = 17 kDa and a PDI

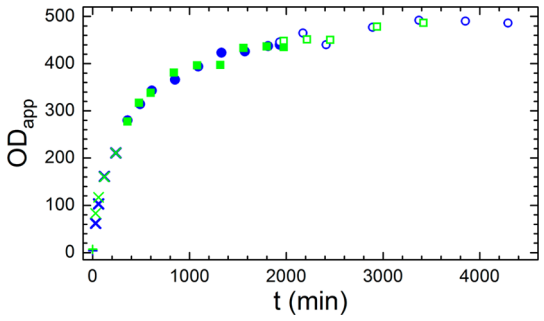

Figure 1. Apparent optical density at 500 nm as a function of strong sonication time for two graphene dispersions, initially 1% by weight in water, and stabilized by the triblock copolymer TB. The initial TB/graphene weight ratio of 0.4 was increased to 0.5 (at about 1900 min). See the Supporting Information for details of power treatments.

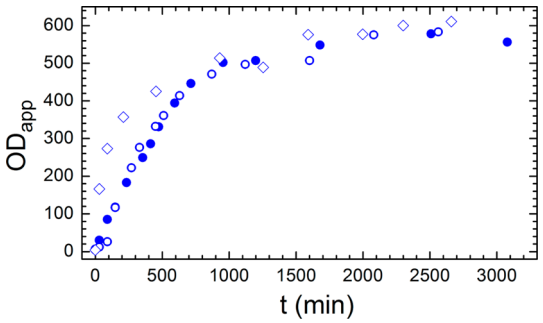

Figure 2. Apparent optical density at 500 nm as a function of strong sonication time for three 1.1% (w/w) graphene dispersions in water that are stabilized by nanolatex NL. In two dispersions (○, ●) the NL:G weight ratio was initially 0.4:1 in NL:G. A third dispersion (◊) was prepared with an NL:G ratio 0.5:1 from the start.

(polydispersity index) of about 1.5. It exhibits an interesting LCST-based phase boundary in water at compositions above 0.31 weight fraction.[87]

Nanolatex was synthesized by microemulsion polymerization in the aqueous−ILBr−MMA ternary system as earlier described.[78,88,89] These lightly cross-linked nanogel particles were in the 20−30 nm diameter size range. They exhibit tunable aqueous stability due to the variable solubility of the imidazolium anion pairs mentioned previously. Such nanolatexes have been found to perform better than a variety of commercially available latexes in coating adhesion; they also form films that can be controllably porated using anion exchange.[89]

RESULTS AND DISCUSSION

Based on our earlier experience with other forms of nanocarbon (carbon nanotubes, fullerene, nanoWC), we used a laboratory-scale moderate power sonication system with a narrow horn (tip ∼3−4 mm diameter). In addition, we maintained the dispersion reactor (∼20 mL glass vial) in an ice bath to mitigate thermal damage. Regev and co-workers[90] and Green and Hersam[91] also used ice-bath immersion as a temperature-control approach in their graphene dispersion experimentation. We started our experimentation at graphene weight concentrations of 1 and 1.1%, respectively, for TB- and NL-stabilized dispersions. We used gravimetry, UV−vis spectrophotometry, and SEM (scanning electron microscopy, Hitachi 3400N) to characterize our dispersions. We did not use centrifugation at any stage of our dispersion processing.

Our dispersion processing for TB-stabilized dispersions is illustrated in Figure 1, where dispersion-apparent optical density at 500 nm is plotted as a function of sonication time. By apparent optical density we mean the optical density that would be measured if the dispersion obeyed Beer's Law and was not so concentrated as to be measurable by ordinary UV−vis spectrometry. These dispersions are actinic, so high dilutions were made (*e.g.*, 500−5000-fold) in order to measure an absorbance in the range of 0.1 to 1 absorbance units at 500 nm. The apparent optical density was then obtained by multiplying this low optical density measured by a net dilution factor for each particular sample.

Our two TB-stabilized dispersions discussed were composed of graphene (G) in water at 1% (w/w) and a TB:G weight ratio of 0.4:1 to 0.5:1. In Figure 1 we see that the apparent optical density (OD_{app}) climbs "quickly" (in less than 5 h) with moderately (50% of maximum amplitude) strong sonication, where a 0.4:1 TB:G weight ratio was used. On increasing the treatment time and intensity (100% amplitude; see the Supporting Information for full details), the OD_{app} more than doubles, but the rate of increase appears to slow over the 1500−2500 min interval and becomes essentially "asymptotic" over the last 2000 min of treatment. We then added an incremental amount of TB, increasing the TB:G ratio to 0.5:1. Over the next 1500 min of sonication the OD_{app} appears to reach an asymptotic limit. The last six OD_{app} values obtained at sonication times greater than 2800 min correspond to an effective absorption coefficient of 48.5 ± 0.6 cm^2/mg (assuming 1% graphene as at the start) at a wavelength of 500 nm. A subsequent gravimetric analysis of this dispersion indicated an increase to 1.69 ± 0.04% solids over the course of this lengthy treatment, resulting in a final graphene concentration of 1.12% (w/w). This increase lowers the apparent absorption coefficient to 43.3 ± 0.5 cm^2/mg. This absorption coefficient is very close to that based on the fine structure constant-based absorption coefficient for graphene (discussed later). The reproducibility of results illustrated in Figure 1 is good, given the concentrated nature of the underlying dispersions. While this good reproducibility is easy to see by inspection of the data in Figure 1, the average percent relative deviation over the 100 min to 3000 min interval is less than 0.8%. The effect of increasing the TB:G ratio from 0.4:1 to 0.5:1 was an increase of about 10.5% in apparent absorption.

The activated exfoliation of several aqueous graphene dispersions stabilized by our NL is illustrated in

Figure 2 where graphene is dispersed at 1.1% (w/w) and NL:G ratios of 0.4:1 and 0.5:1 were used. Two of these dispersions were identically formulated at a 0.4:1 NL:G ratio. Detailed sonication intensities over each treatment interval are provided in the Supporting Information. The dynamical behavior obtained for these two dispersions looks similar to that of Figure 1 in that there is an initial steeply rising interval in OD_{app} followed by an asymptotic interval. This initially steeply rising interval increases about 30% more than the TB-stabilized dispersion of Figure 1, although the graphene concentration in these NL-stabilized dispersions is only 10% greater. It may be that this nanolatex is more effective as a stabilizer in some way. Morphologically, it is certainly different, and each nanolatex spheroid has a radius of 10−15 nm, whereas the radius of gyration of a TB molecule is closer to 3−4 nm.

A third dispersion formulated with 25% more nanolatex than the two discussed above, with an initial NL:G ratio of 0.5:1 produced a faster rise in OD_{app} as can be seen in Figure 2. It is tempting to assign these differences to the increased nanolatex concentration, but a similar experiment done with a 0.4:1 NL:G ratio produced the same initial time behavior for $t < 500$ min. The asymptotic OD_{app} may be slightly higher than for the two other dispersions illustrated, but the differences are not very significant.

Averaging the last seven OD_{app} values obtained at sonication times greater than 1900 min for all three of these dispersions (Figure 2) yields an effective absorption coefficient at 500 nm of 53.0 ± 1.6 cm^2/mg. Evaporation over these processing times resulted in a final graphene weight concentration of 1.19% and a corrected absorption coefficient of 49.0 ± 1.5 cm^2/mg.

More concentrated dispersions stabilized by the same nanolatex were formulated with initial NL:G ratios of 0.4:1 and at 0.5:1 at an initial graphene concentration of 4.0% (w/w). A similarly varied sequence of sonication (see the Supporting Information for details) was applied, and the effective optical density for these two dispersions is illustrated in Figure 3. The dynamical behavior for these more concentrated graphene dispersions in water also appears to exhibit two temporal domains: $t < 1000$ min and $t > 1000$ min. In the first of these dispersions (diamonds and circles; blue online) formulated with a 0.4:1 NL:G ratio, this ratio was increased to 0.5:1 after about 1600 min. This ratio was increased again to 0.6:1 after 5300 min, but no significant gain in OD_{app} was realized. This result implied a 0.5:1 NL:G ratio produced limiting results. The other dispersion (squares; lime green online) was made using an initial NL:G ratio of 0.5:1, and this ratio was not changed thereafter. This second formulation, however, very much duplicates the same behavior derived from the preceding one, and this duplication empirically confirms the exfoliation achieved for 4% (w/w) graphene in water requires an

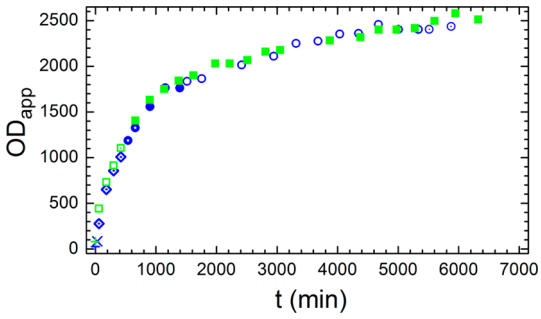

Figure 3. Apparent optical density at 500 nm as a function of strong sonication time for two dispersions initially 4% graphene (w/w) in water and finally 5% (w/w).

NL:G ratio of about 0.5:1. The asymptotic average OD_{app} for $t > 4500$ min yields 48.9 ± 1.2 cm^2/mg as an estimate for graphene's absorption coefficient at 500 nm. Averaging these asymptotic values for the five NL-stabilized dispersions of Figures 2 and 3 yields 48.9 ± 1.3 cm^2/mg, and this value represents a greatest lower bound to the "true" value, as we have not centrifuged or attempted to separate or fractionate our dispersions in any way. We discuss the magnitude of this value later when we compare it to separate measurements obtained on single- and few-layer macroscopic graphene sheets in air. However, these 1−5% by weight graphene in water dispersions are the most concentrated dispersions of graphene in water reported and surpass previous reports of "high concentration graphene"[64] by a factor of up to 166-fold.

We do not have quantitative area exfoliated sheet or few-sheet area distributions as a function of sonication time, but we do know that the initial size of platelets is multimicron and their final size is submicron. A typical comparison is illustrated in Figure 4 where starting material is compared with platelets that had been sonicated for 113 h in a 5.0% (w/w) graphene dispersion. Figure 4a clearly shows platelets with linear dimension in excess of 5 μm. The highly activated and extensively sonicated sample shown in Figure 4b, however, shows that many platelet dimensions are in the submicron range (see the Supporting Information for additional SEM). Sonication is known to sever nanotubes and to "chop" graphene platelets into smaller platelets, and our own SEM studies confirm this effect. It is also known from various processes developed to transform graphite into graphene oxide that the concomitant oxidation of single graphene sheets leads to oxygen-based defects that destroy the visible band structure of graphene.[92,93] We have shown empirically that severe conversion of large platelets to much smaller ones does not significantly destroy the visible absorption of graphene, in spite of extremely lengthy sonication times. We believe that maintaining the processing temperature at about 0 °C greatly contributed to this apparent minimization of oxidative degradation. We further stress that the surface modifications

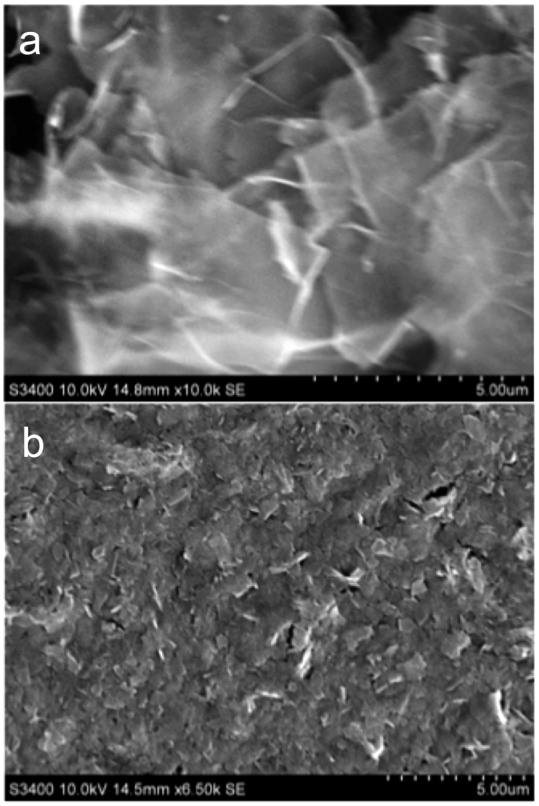

Figure 4. SEM of graphene platelets (a) prior to being dispersed with strong sonication; (b) after sonication for 113 h in 5.0% (w/w) graphene dispersion.

demonstrated here are ones of physical adsorption, rather than covalent functionalization that also disrupts band structure.

Disparity between TB-Stabilized and NL-Stabilized Results. The absorption coefficient derived from our TB-stabilized dispersions is about 10% lower than those seen for these NL-stabilized dispersions. This disparity is over 5-fold more than the uncertainty associated with experimental reproducibility. Our current hypothesis is that the TB molecules, to a certain limited extent, create metastable few-sheet platelets and turbostatic[1] bilayers.

Metastable few-sheet platelets are envisioned to have TB molecules adsorbed simultaneously to both outer surfaces of a few-sheet platelet, where a TB molecule wraps around platelet edges. The end-to-end length of a TB molecule is about 20 nm (almost the diameter of a nanolatex particle). We would, therefore, expect that near-edge adsorption of a TB molecule could lead to the molecule wrapping around the platelet edge and contacting the opposite side.

Turbostatic bilayers are envisioned to be two-sheet platelets with a single layer of TB molecules intercalated between two sheets, as well as form a saturated monolayer on both outer surfaces of a bilayer. In such a turbostatic bilayer, each TB molecule between the respective sheets would be strongly bound to both interior graphene surfaces. Both the poly(propylene oxide) groups and the imidazolium bromide groups would be expected to exhibit such adsorption. Turbostatic bilayers have been hypothesized to form in aggregation kinetic studies of sodium cholate-stabilized graphene sheets.[1]

TABLE 1. Storage Stability of TB- and NL-Stabilized Graphene Dispersions

			absorption coefficient (cm^2/mg)	
stabilizer/ graphene (%)	treatment	OD_{app} (500 nm)	after half-year storage	initial
TB/1.12%	2 min vortex mixing	489	43.7	43.3 ± 0.5
NL/1.19%	60 min ultrasonic bath	575	48.3	49.0 ± 1.5
NL/5%	30 min ultrasonic bath	2526	50.5	48.9 ± 1.2

Long-Term Stability. The storage stabilities of these dispersions were checked after about a half year of storage at ambient. The results are summarized in Table 1 (see the Supporting Information for details). In each case, only vortex mixing or mild sonication was required to recover absorption coefficients within 1−1.4 standard deviations of those determined when the respective dispersions were made.

Reasons for this excellent stabilization emanate from three factors: (1) strong van der Waals interactions between the graphene sp^2-delocalized π electrons, underlying sp^2-based σ-bonding orbital electrons, and the $1s^2$ carbon core electrons with the poly(propylene oxide) segment bonding and nonbonding electrons; (2) high affinity of the imidazolium bromide group for nanocarbon and graphenic surfaces due to favorable overlapping of the respective π-systems and due to nonspecific bromide adsorption,[94] affording some attachment to graphene; (3) high affinity for water of imidazolium groups not attached to graphene surfaces and free pendant blocks provide steric stabilization. In this system, we would regard the contribution (1) of the poly(propylene oxide) segments to be the dominant mode of attachment between TB and graphene surfaces. The adsorption from solution of the TB produces graphene surface coatings of osmotic brushes. The adsorption from suspension of the nanolatex produces graphene surfaces coatings of osmotic spheres that, when adsorbed, provide an osmotic brush surface. Osmotic brush coatings are essentially the most effective kinds of steric stabilization one can devise. These dispersions are thereby immunized against destabilization produced by indifferent electrolyte ionic strength fluctuations.

Concentration by Evaporation. The increase in concentration attributed to evaporation was noted in each of these lengthy regimens of sonication at 0 °C, and gravimetric measurements indicated quantitative increases in dispersed graphene amounts of about 8, 12, and 25% on a weight basis, respectively, for our TB- and

NL-stabilized dispersions. These increases are approximately linear in sonication time. While we do not want to unfairly attribute these successes in dispersion to our novel stabilizers, these same stabilizers must be credited with the very long time stability measured after 6−7 months of quiescent storage at room temperature discussed above. Concentration by evaporation is often done by design, as in volume reductions under reduced pressure, *etc*. In our processing it was incidental, but none the less significant (an effect beyond experimental uncertainty).

Effects of Sonication on Polymer Integrity. Another issue of importance associated with sonication effects is the degree to which the stabilizing polymers are degraded by sonication. A study by Arakawa and co-workers of poly(ethylene oxide)−poly(propylene oxide) (PEO−PPO) comonomers indicated that PEO segments were more susceptible to ultrasonic-induced scission and that PPO−PEO junctions were highly susceptible to scission.[95] Other studies of polyvinylpyrrolidone,[96] poly(methyl methacrylate),[97,98] poly(ethyl methacrylate),[98] poly(butyl methacrylate),[98] and poly(acrylic acid)[99] suggest large molecular weight polymers can be degraded into 10^4-10^5 Da fragments by sonication in solution. We found[84] in examining the efficacy of ILBr monomers, homopolymers, and random copolymers, in addition to the nanolatexes and triblock copolymers described here, that all of these stabilizers worked well for producing nanocarbon dispersions. We did not analyze our dispersions for polymer degradation or if adsorbed polymer is degraded more or less than solution or nonadsorbed polymer. However, physical studies should be performed in the future, in conjunction with also trying to quantify the dynamics of graphene sheet scission into smaller dimension sheets.

The efficacy of these stabilizers, in view of likely chain scission processes, is even more noteworthy when we consider the stoichiometries involved. The weight ratio of 0.5:1 of stabilizer to graphene, if we assume complete exfoliation into single sheet graphene, corresponds to (500 mg of polymer stabilizer)/(g of graphene) × (7.604×10^{-8} g of graphene/cm^2 graphene) × (10^4 cm^2/m^2) × (1 graphene sheet/2 sides graphene) = 0.19 mg polymer/m^2 graphene surface. This amount is equivalent to ∼0.5 μmol/m^2 if we assume the stabilizers were ILBr homopolymers, or ∼0.3 stabilizing monomer units/nm^2, or about 330 Å^2/monomer unit. This approximation is a reasonably sparse packing density.

Optical Absorption of Graphene Sheets. A simple model for the optical absorption of graphene in the visible region has been put forward by Nair and co-workers.[100] This model shows that the single layer optical absorption of graphene is provided by graphene's fine structure constant $e^2/\hbar c$, where e is electronic charge, $\hbar$ is Planck's constant divided by 2π, and c is the speed of light.[101,102] This parameter describes the interaction of white light with relativistic electrons, and it provides a wavelength-independent transmittance through the visible, $1 - \pi e^2/\hbar c = 0.9771$. This transmittance represents a 2.29% attenuation by a single graphene sheet. This fine structure constant-based absorption provides an absorption coefficient for light polarized parallel to the graphene surface.[103,104] The optical density (absorbance), $-\log[1 - \pi e^2/\hbar c] = -\log[0.9771] = 0.01006$, may be expressed as the product of an absorption coefficient, $\alpha_{\|}$, a path length (graphene layer thickness, 0.335 nm), and graphene concentration. In order to obtain an absorption coefficient in units of cm^2/mg, we divide the absorbance, 0.01006, by 7.604×10^{-5} mg/cm^2, the areal mass density calculated for a carbon−carbon bond length of 0.1421 nm. We therefore have $\alpha_{\|} = 132.3$ cm^2/mg. A graphene sheet thickness of 0.3354 nm,[104] corresponding to sheet separation distances in crystalline graphite, yields a calculated density of 2.269 g/cm^3. Surface graphite layers would be expected to have a slightly greater separation, and isolated graphene layers would be expected to be thicker still. Estimates of graphene layer thicknesses of 0.08 nm,[105] 0.10 nm,[106] 0.34 nm,[107] 0.351 nm,[108] 0.37 nm,[109] and 0.38[110] nm have been reported as a result of various ellipsometric fitting models.

Electronic structure studies of graphene indicate only visible light that is plane-polarized can be absorbed by graphene. Perpendicularly polarized light (with respect to the graphene plane) is not absorbed by graphene.[103,111] This selection rule yields the following relation for absorption coefficients measured for randomly ordered platelets of graphene:[112]

$$\langle\alpha\rangle = \frac{1}{3}\alpha_{\perp} + \frac{2}{3}\alpha_{\|} \quad (1)$$

When $\alpha_{\perp}$ vanishes, the experimentally measured absorption coefficient is:

$$\langle\alpha\rangle = \frac{2}{3}\alpha_{\|} \quad (2)$$

Taking $\alpha_{\|} = 132.3$ cm^2/mg then yields $\langle\alpha\rangle = 88.2$ cm^2/mg, for absorbance emanating from intraband $\pi \rightarrow \pi^*$ transitions (fine structure constant band). There are two contexts in which to discuss this "excess" absorption. One is that a variety of experimental studies unequivocally suggests the visible absorption of graphene exceeds that predicted by the fine structure constant.[109,113,114] A second is that the selection rules governing the vanishing of $\alpha_{\perp}$ change due to symmetry lowering and breaking imposed by vibronic perturbations to the electronic structure.[115−118]

The basis for the absorbance emanating from the fine structure constant process described above emanates from a $\pi \rightarrow \pi^*$ valence to conduction intraband transition. While this component is predicted to be

invariant with frequency, dramatic decreases in the infrared and gradual to large increases through the visible to UV have been unequivocally observed in graphene and in graphite. The main source of increase above 1 eV can be assigned to an excitonic resonance at 4.62 eV, and the data of Weber *et al.*[107] indicate an absorbance (0.01173 ± 0.00010) at 2.48 eV (500 nm), 16.6% higher than that from the fine structure constant (0.01006). The experiments of Nair and co-workers show a very similar deviation above 2 eV in the absorbance (see their Supporting Information[100]), but not to the same extent. The data of Gray *et al.*[110] indicate a much greater departure with increasing energy. At 500 nm their transmittance of 0.9679 corresponds to an absorbance of 0.01417 (20% greater than the Weber *et al.* value[107] and 40.9% greater than the fine structure constant value).

These intraband transition and excitonic processes occur only for excitations driven by light-polarized parallel to the graphene plane. Certain vibronic effects might be expected to make the vanishing transition dipole moments with perpendicularly polarized light become allowed. Flexural phonons have been discussed and are of various types.[119] Those that result in bending graphene lift (break) planar symmetry and would be expected to result in additional oscillator strength for these same transitions. Thermally induced out-of-plane oscillations of trigonal carbon atoms would be expected to do the same. Since room temperature corresponds to the thermal energy of about 29 meV, such flexural phonons should be expected to be contributing to the experimental absorption of graphene in suspension, if not on a solid support.

Another source of oscillator strength may be expected to arise from edge electronic states around the periphery of monolayer or few-layer graphene sheets in suspension. Such states do not exist in infinite 2D graphene, but are expected in any dispersed form of graphene and have been described, at least in part, geometrically. A 1 μm square graphene flake would have at least 0.01% of its carbon atoms at flake edges with dangling bonds (methine bonds to hydrogen or unknown oxidation state). Decreasing the size of such flakes to 100 nm squares results in a 100-fold increase in the number of edge carbon atoms. Such fragmentation is certainly within the realm of practicality as shown in Figure 4 (and in SEM of the Supporting Information).

In view of the available optical absorption data for graphite and graphene, our average absorption coefficient $\langle\alpha\rangle$ = 48.9 ± 1.3 cm^2/mg is consistent as a greatest lower bound to 103 cm^2/mg (2/3 $\alpha_{\|}$) with the analyses of Nair *et al.* in view of Weber *et al.*[107] ($\alpha_{\|}$ = 154 cm^2/mg at 500 nm). In view of the various mechanisms that lift the $\alpha_{\perp} = 0$ "selection rule" and that are expected to be active especially in the production of aqueous dispersions, we believe each of the values derived in our separate dispersion series represent lower bounds and are not necessarily the ultimate values. Reference values for monolayer and multilayer graphene/graphite, however, exhibit quite a bit of variability, as can be seen in the comparison given in Weber *et al.*[107] (Figure 3 therein) and in Matkovi *et al.* (Figure 4b therein).[122] We consider that, at present, the results of Weber *et al.* are the best available results, basically because they did not fix the thickness of single-sheet graphene to the crystalline graphite value, but derived a thickness of 0.34 nm from their fitting, 1.5% greater than that of crystalline graphite.

The compilation[116,121] available in Matkovi *et al.*[122] indicates an absorbance at 500 nm of 0.0129 and a corresponding $\alpha_{\|}$ = 169 cm^2/mg at 500 nm ($\langle\alpha\rangle \sim$ 56.6 cm^2/mg). These results appear founded on an assumed sheet thickness of 0.335 nm. The results of Chae *et al.*,[123] from confocal microscopy, suggest an even stronger absorbance at 500 nm and a bilayer absorbance 2.7-fold larger than that of a single layer. Similarly, detailed examination of the calculated results of Yang *et al.*[120] (see Figures 2 and 4 therein) yields 60.9 cm^2/mg for $\langle\alpha\rangle$, and the bilayer (constrained to have bulk graphite interlayer spacing) absorbance at 500 nm is 2.36 that of the single sheet. The calculated dielectric loss intensity also exceeded the measured value by about 17%, suggesting the calculated $\langle\alpha\rangle$ should be about 106 cm^2/mg. The range of 103 to 113 cm^2/mg for $\langle\alpha\rangle$ that exists in ellipsometric, confocal, and theoretical determinations corresponds to an uncertainty of about 10% that may be attributed to not having an unequivocal measurement of single-sheet graphene thickness. In view of the historical difficulties involved in "seeing" graphene sheets, this issue might best be answered by an extensive theoretical analysis of the protrusion of $2p_z$ electron probability distributions on either side of the carbon plane.

The selection rules discussed above indicate that the absorption coefficients measured in graphene dispersions should be multiplied by 3/2 to properly compare to oriented single-sheet absorption studies. It appears the absorption coefficients we measured for our NL-stabilized dispersions are about half of what we would expect from the single-layer measurements of Weber *et al.*,[107] wherein both excitonic and hyperfine structure constant[100] mechanisms of absorption are important. A possible cause of this disparity may be unquantified oxidative damage to the graphene π system (which would tend to lower visible extinction). Further work is clearly needed to quantitatively connect dispersion results to macroscopic single-sheet work.

Comparison with Previous Dispersion Estimates. Estimates of optical absorption coefficients for graphene in dispersion have been derived from mild sonication studies of graphene supernatant suspensions by various groups in different solvents. Comparison of various experimental and theoretical spectra indicates that $\langle\alpha\rangle_{660\ nm}$ is 85% of $\langle\alpha\rangle_{500\ nm}$. Values for $\langle\alpha\rangle$ at 660 nm (1.89 eV)

reported by other groups have included 7.1 cm^2/mg (in aqueous sodium cholate by ICl intercalation, thermal expansion, and homogenization),[1] 9.3 cm^2/mg (in DMF by comminution),[53] 11.7 cm^2/mg (in 1-hexyl-3-methyl imidazolium PF_6^-),[65] 13.9 cm^2/mg (in water),[124] 24.2 cm^2/mg (in 3-glycidoxypropyl trimethoxysilane),[125] 24.6 cm^2/mg (in NMP, *N,N*-dimethylacetamide, γ-butyrolactone, and 1,3-dimethyl-2-imidazolidinone[59] and applied to aqueous dispersions[91]), 36.2 cm^2/mg (in NMP),[51] 47.1 cm^2/mg (in phenyl triethoxysilane),[125] and 66 cm^2/mg (in water).[64] The three absorption coefficients determined in water, 7.1, 13.9, and 66 cm^2/mg, are too small or too large to be consistent with the fine structure constant, intraband transition results of Nair and co-workers, corresponding to 8.0%, 15.8%, and 74.8%, respectively, of their 88.2 cm^2/mg value. It is difficult to be certain about this extremely large variability. Many of these measurements were based on measuring dilute dispersions of single-sheet through multisheet graphene flakes, and in these situations we believe the full optical absorption is suppressed by intersheet interactions. In addition, we have no general understanding of the expected effects of surface solvation on the respective transition moments.

These previous studies show unequivocally that the absorption coefficients of few to multisheet graphene flakes are significantly less than the greatest lower bounds of 42 cm^2/mg at 660 nm or 48.9 cm^2/mg at 500 nm and the ranges of 88−90 cm^2/mg at 660 nm and 102−106 cm^2/mg at 500 nm from ellipsometry[107] and theory.[123] Hopefully, flake thickness distributions[49,91] will be coupled with single-flake absorption measurements at some point in the near future.

These comparisons indicate the generally accepted value of about 24.6 cm^2/mg at 660 nm should be replaced by the higher value, 88 cm^2/mg (103 cm^2/mg at 500 nm).[100] The disparities that exist underline the importance of further work on single- and few-sheet flakes and on so-called graphene "quantum dots," so that we better understand sheet-thickness effects and how optical properties are transformed by the transition from infinite 2D properties to supramolecular 2D quantum dots.

Layer-by-Layer Assembly. A layer-by-layer (LbL) approach[126,127] was used to examine the efficacy of the sonication-driven exfoliation processing. LbL coating methods use alternating deposition of cationic and anionic polyelectrolytes or other charged nano-objects to prepare multilayer coatings and materials. We used a solution 1% (w/w) in sodium polystyrenesulfonate and a 1.4% (w/w) dispersion of NL-stabilized graphene in water to prepare series of bilayer coatings on 1 in. × 3 in. microscope slides. After every sixth bilayer, the slides were examined by visible absorption spectrometry, and the resulting data for two sets of coatings are illustrated in Figure 5. Linear regression was then used to fit the data to a straight line and a slope of

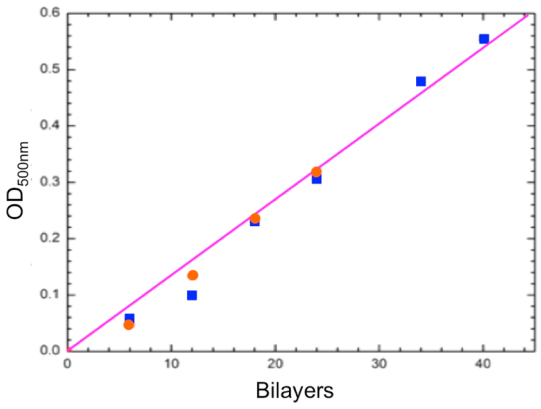

Figure 5. Optical absorption at 500 nm of glass slide coated sequentially with bilayers of sodium polystyrenesulfonate and NL-stabilized graphene. The data points correspond to two different series of LbL coating series, and each is an average of three measurements made at different locations on the slides. The line with slope 0.0135 OD/bilayer represents a linear regression fit to the data points constrained to pass through the origin.

0.0135 OD/bilayer was obtained. When this slope is divided sequentially by three times the apparent absorption coefficient measured in dispersion (3/2 × 103 cm^2/mg = 154 cm^2/mg), the effective density of monolayer graphene (7.604 × 10^{-5} mg/cm^2), one obtains 0.77 graphene sheets/bilayer. This result suggests the exfoliation process for these nanolatex stabilized dispersions is nearly complete.

We always saw a significant expansion of the graphene mass in the reactor immediately after the ultrasonic bath treatment, and we consider the activation for this pretreatment process to be small. We believe exfoliation commences with n-sheet flakes being separated into (*n*−*r*)-sheet and *r*-sheet flakes. These flakes are sequentially separated into smaller flakes until only few-sheet flakes and single sheets remain. We postulate that the exfoliation of two-sheet and three-sheet platelets is more highly activated than exfoliation of 5-sheet to 35-sheet platelets. It would be very helpful to have a thickness mass distribution for these dispersions of the type generated by Colman and co-workers[49] and by Green and Hersham.[91] We know from the transmission data of Nair *et al.* that the transmittance of multilayer graphene begins to deviate from the fine structure constant value for three layers and greater, and it is reasonable to believe further that the absorption contribution of excitonic-based excitations may be affected by sheet packing. We also know from all of the earlier estimations of visible absorption coefficients for graphene that mixtures of single-sheet through 10-sheet graphene platelets have absorption coefficients significantly less than that we report.

The highly activated nature of exfoliation suggests stabilizer intercalation during exfoliation as the rate-determining step(s). Stabilizer adsorption and surface saturation are processes that affect dispersion stability.

It has been repeatedly pointed out that lengthy and high-power sonication fractures graphene platelets into areally smaller platelets, and our SEM data of Figure 4 (see also the Supporting Information) confirm this behavior. The fact that the optical effective absorption as measured by OD_{app} at 500 nm essentially climbs to an experimentally asymptotic value argues empirically against significant oxidation of the type imposed by extensive oxidation by nitric acid and other oxidants that destroy the band structure of graphene[92] (and of carbon nanotubes[128]). While cutting large sheets into smaller ones certainly increases the population of edge defects, it does not block these dispersions from being the most concentrated in graphene produced in water, while simultaneously exhibiting visible absorption more closely in agreement with single-layer graphene studies.

Simply cleaving sp^2 σ bonds is not expected to deplete the electron occupancy of the $2p_z$ atomic orbitals responsible for both the intraband a $\pi \rightarrow \pi^*$ and excitonic transitions responsible for the observed absorption in the visible. Simply severing these sp^2 sigma bonds would increase the number of nonbonded electrons, as would any accompanying oxidation process, whether in the formation of aldehyde, hydroxyl, or carbonyl groups. It is interesting to ponder if excitations emanating from such nonbonding electrons might provide additional finite transition moments that would increase the $\alpha_\perp = 0$ component of the absorption coefficient. Nonbonded electrons that are not confined to the graphene plane might generate noticeable oscillator strength. However, the increase in platelet perimeter on going from 4.5 μm $\times$ 10 μm platelets to 500 nm $\times$ 500 nm platelets (2 μm/29 μm $\times$ 45 μm^2/0.25 μm^2) is a factor of about 12. Such defects, therefore, may account for some of the apparent absorption intensity, although our experimental values do not exceed those reported for single-layer graphene by Weber and co-workers.[107]

Kinetics Scaling. Each of the experimental OD_{app} vs time plots in Figures 1−3 exhibit two apparent domains of behavior, a quickly rising component followed by a much more slowly rising, asymptotic component. When analyzed according to $OD_{app} \sim t^{\beta}$ (see the Supporting Information), these scaling exponents β are determined from the slopes of log−log plots. In each case two linear intervals are seen. A summary of these exponents is given in Table 2. These scaling exponents exhibit some apparent consistencies and inconsistencies. In the first interval, $\langle\beta\rangle_{first} = 0.55 \pm 0.22$. In the second interval, $\langle\beta\rangle_{second} = 0.20 \pm 0.02$ and is more uniform than in the first interval. The first domain $\langle\beta\rangle$ value suggests diffusion is an integral component of the exfoliation occurring in the first interval. The second domain $\langle\beta\rangle_{second}$ = 0.20 value suggests this more lengthy process is more highly activated than the first domain process. The average value of 0.55 in the first interval is approximately that expected for a diffusion controlled process, and within experimental uncertainty matches a similar result obtained by Coleman and co-workers.[51,55]

TABLE 2. Exfoliation Scaling Parameters

	β	
dispersions	first interval	second interval
1% TB	0.52	0.17
1.1% NL	0.86	0.19
1.1% NL-100[a]	0.35	0.20
4% NL	0.47	0.22

[a] Dispersion formulated initially 0.5:1 in NL:G (in Figure 2).

Upon application of medium- to high-power sonication, we see the evolution of two behavior domains, where both are apparently dominated by first-order kinetic-diffusion processes. We can write processes of deaggregation and exfoliation from such aggregates to stabilized individual graphene sheets as a sequence of first-order processes:

$$[G_n]_m \rightarrow mG_n \rightarrow mG_{n-r} + mG_r \rightarrow \cdots \rightarrow \cdots \rightarrow (mn)G_1 \quad (3)$$

In this hypothesized mechanism, multisheet aggregates, G_n, split (exfoliate) into a pair of thinner sheets. A detailed and quantitative analysis of these data in terms of such a model will be presented in a subsequent paper. The impact of stabilizer type and concentration is seen indirectly in such a model (for example, in terms of pseudo-first-order rate constants).

Rheo-optical Fluids. These graphene dispersions, dilute or concentrated, are rheo-optical fluids. Although graphene is believed to have low reflectivity,[129−131] we demonstrate an interesting constructive reflectance phenomenon in Couette shear fields. A 1.19% (w/w) graphene dispersion is illustrated in Figure 6a, where the illumination is predominantly upon the front of this sample vial. Note that a cylindrical stirrer of about 9 mm diameter is centered in the vial. Most of the reflected light seen in Figure 6a is being reflected from the outer and inner glass surfaces of the vial. The image in Figure 6b is different, and in this case, the stirrer is being rotated at 1000 rpm. This rotation speed and the barrel and vial dimensions indicate the shear field established is about 70 s^{-1} over the 0.6 cm between the rotation barrel surface and the inside of the vial. This shear field sets up a series of Couette convective cells, and in the frame illustrated, whitish bands appear due to constructive reflectance from shear-aligned graphene sheets. This shear alignment emanates from the shear field established by this Couette form of mixing, wherein velocity increases from near zero at the inner glass surface to near that of the rotating barrel surface. Several video clips illustrating this rheo-optical effect are available in the Supporting Information.

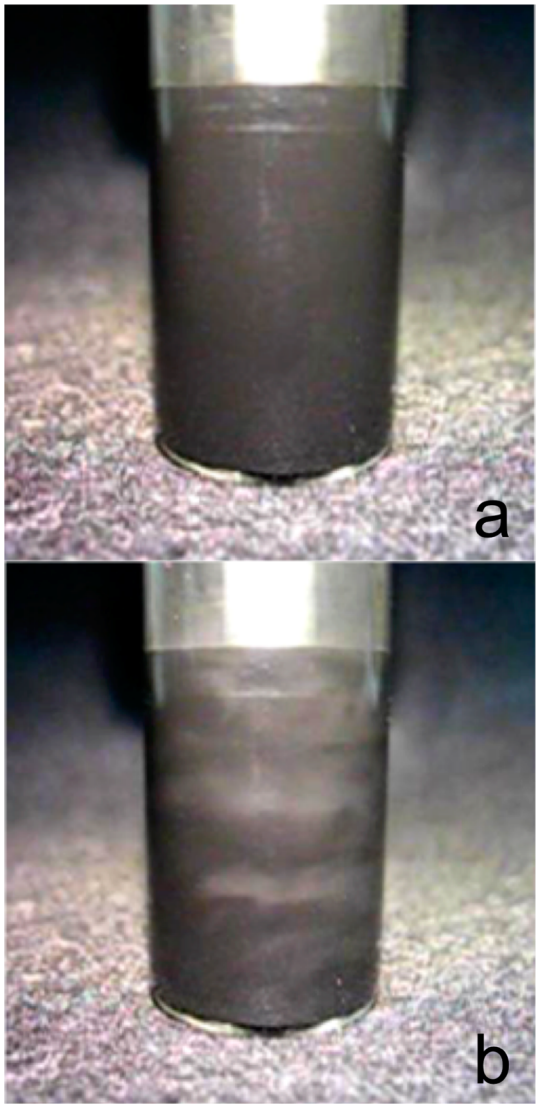

Figure 6. Photograph of vial containing 1.1% (w/w) NL-stabilized graphene dispersion with aluminum cylindrical stirrer (a) at rest and (b) at 1000 rpm. This change in reflectivity illustrates an isotropic to nematic transition.

This kind of shear alignment is referred to as an isotropic to nematic transition, where the "nematic" orientation produces constructive reflectance. While it is known that shear fields align platelets,[132−136] we have not succeeded in finding a reference reporting being able to detect this phenomenon visually in room light as is illustrated in Figure 6. A rationalization for this paucity of earlier reports may be that dispersions of clays and other disklike materials will tend to be milky and opaque to the eye if the platelets are big enough to scatter visible light, and the marginal increase of scattering on alignment may not be so obvious, as it is in this case where the constructive reflectance is cast against an actinic (black) background.

Stimuli-Responsive Phase Transfer. Both this nanolatex and this triblock copolymer have been found to exhibit interesting stimuli-responsive behavior in response to

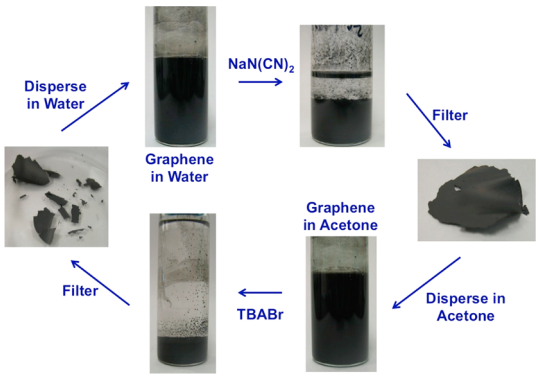

Figure 7. Solvent-transfer cycle from water to acetone and back to water. A stable aqueous dispersion is destabilized by addition of $NaN(CN)_2$, filtered, redispersed in acetone, destabilized by addition of TBABr, filtered, and then redispersed in water.

certain types of anions. We show in Figure 7 for TB-stabilized graphene (and in the Supporting Information for NL-stabilized graphene) that this stimuli responsiveness can be used cyclically to effect phase transfer from water to organic solvent (acetone) and back to water. A stable aqueous graphene dispersion is easily destabilized by addition of sodium dicyanoimide. The anion exchange of Br^- for $(CN)_2N^-$ switches the water-loving (hygroscopic) imidazolium bromide groups in the TB-stabilized graphene dispersion to being hydrophobic. The resulting flocculation and sedimentation allows the graphene to be collected by filtration, washed, and dried to form a graphene paper. The paper obtained after filtration is wrinkled because it was dried without maintaining any in-plane tension or compression normal to the plane. Similar papers derived from graphene by simple filtration have also been documented.[137,138] This paper was then crumbled, placed in acetone, and mildly sonicated to produce a stable graphene dispersion in acetone. This dispersion was then destabilized by adding an excess of tetrabutylammonium bromide, after which the bromide anion exchanges with the dicyanoimide and aggregation and precipitation of the graphene in the acetone. The destabilized and sedimented graphene was then filtered, rinsed and dried. It was then redispersed in water with mild sonication, completing the cyclical phase-transfer process.

This kind of stimuli-responsive phase transfer was first demonstrated by the group of Mecerreyes,[139] where a homopolymer (PIL, polymerized ionic liquid) of an ionic liquid monomer, 1-vinyl-3-ethylimidazolium bromide, was used to stabilize dilute SWCNT in water and anion exchange of bromide for $(CF_3CF_2SO_2)_2N^-$ (Pf_2N^-). The bromide form of the polymer provides excellent stabilization in water but poor stabilization in acetone. The Pf_2N^-, after displacing Br^-, provides good non-aqueous solubility. Kim and co-workers[140] used the same homopolymer to stabilize graphene oxide (GO) in water (<0.15% w/w GO) and found that the reduced

graphene oxide (rGO) remained stabilized in water after chemical reduction. They then demonstrated that anion exchange of the Br^- with $(CF_3SO_2)_2N^-$ (Tf_2N^-) effected restabilization of the rGO in propylene carbonate. Yuan and co-workers similarly demonstrated graphene phase transfer using a tetrabutylphosphonium poly(ionic liquid) stabilizer.[141]

Such phase transfer or solvent transfer is important because it dramatically increases the practical application of such dispersions. A dispersion may easily be prepared at high concentration in water and stored until needed. Ion exchange can then be used to make the dispersed phase highly hydrophobic but easily redispersed in an alternative solvent or even a water immiscible monomer. This property therefore provides practical means to preparing a wide range of composite materials.

Summary. We have found that these IL-based triblock copolymer stabilizers and IL-based nanolatexes are excellent stabilizers for graphene in water. We have argued that the delocalized π system of the imidazolium groups provide a simple mechanism to account for how these backbone groups physically adsorb to graphenic sp^2 surfaces.

While these 1−5% by weight graphene dispersions are the most concentrated reported to date for graphene in water, surpassing previous "high concentration" results by 2 orders of magnitude, we believe higher concentrations are feasible. It has been hypothesized that greater than 10% by weight dispersions may be possible, but at some stage intersheet attractions and repulsions are expected to produce untoward viscosity limitations.[142]

Our optical density studies have illustrated higher absorptions in the visible for dispersed graphene than has previously been realized. Comparisons with fundamental oriented optical studies of graphene and with graphite have allowed us to draw a very close connection between our dispersion results and those more fundamental single-sheet and few-sheet results. Our absorption coefficient results (in dispersion) are greatest lower bounds to the presently most reliable single-sheet results. Our LbL experiments independently support the self-consistency of our optical interpretation.

Scaling analyses provide strong evidence that the kinetics of exfoliation are diffusion controlled. We hypothesized a diffusion-controlled sequential irreversible exfoliation mechanism.

We demonstrate that such graphene dispersions are rheo-optical fluids and that simple Couette shear fields can be used to align micron and submicron sheets over macroscopic areas. Such behavior is expected to lead to excellent coating effects in future moderate shear-coating applications.

The stimuli responsiveness to various anions that has been illustrated in various contexts earlier for these same stabilizers has been used to show that graphene dispersed in water, as demonstrated here, may be transferred to nonaqueous media and easily redispersed. This characteristic greatly broadens the range of applications that may be envisioned for such dispersions, particularly in composite materials formulation.

These aqueous dispersions are suitable as conducting inks as made in these experiments. They can be loaded and dispensed by extant writing devices such as ink jet and related methods. They can also be applied using diverse coating methods. Kinetic modeling of these data and various coating applications will be addressed in forthcoming papers.

MATERIALS AND METHODS

Materials. Graphene as platelets 1.5−10 μm in lateral dimension, comprising about 20−50 graphene layers (sheets) and about 12 nm thick, was obtained from the Graphene Supermarket (Reading, MA; http://graphene-supermarket.com) as grade AO-3. This powder was ground by hand with an agate mortar and pestle before use.

The triblock TB was synthesized using ATRP (atom-transfer radical polymerization) to grow ILBr end blocks from a macroinitiator of 3500 Da poly(ethylene oxide)-di-OH, as described previously.[87] Nanolatex was synthesized by microemulsion polymerization in the aqueous-ILBr-MMA ternary system as described previously.[78,88,89]

Sonication. Mild sonication was done with an ultrasonic cleaning bath (Branson Model B300, Danbury, CT) for various time periods as needed. Stronger sonication was done with a sonifier using a microtip sonic horn about 3−4 mm diameter at the tip end (SONIS Vibra Cell, Model VC 30, Newtown, CT). The reactor was held in an ice−water bath using a clamp. Sonication was done over extended time periods. Prior to strong sonication, a dispersion would be sonicated in the cleaning bath for 60 min at the beginning of the dispersion process or for 30 min after an overnight or longer rest period. The dispersion plus reactor (vial) were weighed at the beginning and at the end of every extended sonication treatment. This was to keep track of mass loss due to evaporation, due to sonic ejection of microscopic droplets, and due to aliquots withdrawn for analysis of apparent optical density. Aliquots of 30−50 μL were withdrawn and placed in a tared vial and then diluted one or more times to obtain a dilution having an absorbance at 500 nm or at 660 nm in the desired range. The sonifier horn tip was placed about 1 cm above the bottom of the reactor for strong sonication.

Optical Absorption. Spectra at a fixed wavelength were measured with a JASCO V-530 UV−vis spectrophotometer using a tungsten bulb as light source. Graphene dispersion samples were diluted (by weight) sufficiently to obtain absorbance values in a range of about 0.1−1.0.

Microscopy. SEM (scanning electron) was done with a Hitachi S-3400N VP instrument (Hitachi America, Pleasanton, CA). Optical microscopy was done with a Zeiss research grade optical microscope (Carl Zeiss Microimaging Inc., Tornwood, NY).

Layer-by-Layer Assembly. Glass microscope slides (1 in. × 3 in.) cleaned in ethanol were placed in a UV/ozone cleaner for ~30 min to 1 h on each side. A solution of 1% (w/w) poly(sodium 4-styrenesulfonate) and a suspension of NL-stabilized graphene about 0.4% (w/w) were prepared. A slide was first placed into the graphene suspension and allowed to soak for 5 min; it was then rinsed by dipping in three successive beakers of DI H_2O.

The slide was then dried in an oven at 70 °C and then placed in the PSS solution for 5 min and rinsed and dried as described above. This process was repeated cyclically for a desired number of bilayers. Optical absorption measurements were made after every third cycle (six bilayers); bilayers were coated simultaneously on both sides of each slide. Three absorption measurements, each at a different location on the slide, were made and the resulting averages are depicted in Figure 5.

Couette Shear. This cylindrical rod stirrer was an aluminum barrel of an Exacto-knife assembly, and it is mounted in a digitally controlled mixer chuck.

Phase Transfer. (See the Supporting Information for complete details.) A TB-stabilized dispersion that had been stored at room temperature for 20 months was vortexed and then sonicated in a cleaning bath for 30 min. An aliquot produced an OD_{app} of 499 at 500 nm that indicated an absorption coefficient of 44.6, in good agreement with the 43.3 ± 0.5 cm^2/mg obtained 20 months earlier (and 3% higher!). This dispersion was combined with an equal volume of 1 M $NaN(CN)_2$ (in order to destabilize the dispersion) and allowed to sediment gravitationally overnight. The sediment was filtered, washed three times with water, and dried. An acetone dispersion was prepared by diluting dried sediment with acetone. This dispersion was vortexed and placed in an ultrasonic cleaning bath for 30 min. It was then sonicated at successively higher power settings. The total solids concentration was 0.949%, and the graphene concentration was 0.67%. An analysis of an aliquot of this dispersion yielded an OD_{app} of 343.6 that corresponds to an absorption coefficient of 51.3 cm^2/mg, near the limits suggested by the data of Weber *et al.*[107] and the calculations of Yang *et al.*,[120] and significantly higher than the 43.3 cm^2/mg estimated 18 month earlier. About 5 mL of 0.5 M TBABr (tetrabutylammonium bromide) in acetone was added to TB-stabilized graphene dispersion in acetone. The dispersion was destabilized, and the graphene dispersion was destabilized by the replacement of $(CN)_2N^-$ with Br^-. The sedimented solids were collected by filtering and washed three times with acetone, and then the graphene covered filter was placed in an oven at 75 °C to dry overnight. The dry graphene "paper" was separated from the filter, and 35.4 mg of solids was recovered. This solid material was crumbled, placed in a vial with 7.6516 g of water, and sonicated in a cleaning bath for 30 min. This dispersion was then sonicated with strong sonication for 1 h at 75% amplitude (11 W output) and then for 2 h at 100% amplitude (18 W output). An aliquot was analyzed and yielded an OD_{app} of 174. This value implies an absorption coefficient of 52.7 cm^2/mg, substantially in agreement with the value of 51.3 cm^2/mg measured earlier.

Conflict of Interest: The authors declare the following competing financial interest(s): J. Texter has an equity interest in a pending US Patent Application US 2011/0233458 A1, Nanoparticle dispersions with ionic liquid-based stabilizers.

Supporting Information Available: Additional details of dispersion preparation, SEM analyses, long-time stability, derivation of anisotropic absorption coefficient components, scaling analyses, videos illustrating shear alignment effects of graphene rheo-optical fluids, and stimuli-responsive phase transfer cycling of NL-stabilized graphene dispersions. This material is available free of charge *via* the Internet at http://pubs.acs.org.

Acknowledgment. This paper is dedicated to Professor Markus Antonietti, whose stimulation and suggestion to one of us (J.T.), during a sabbatical in Golm, at the Max Planck Institute for Colloids and Interfaces, to use these nanolatexes to disperse CNT in water resulted also in the application detailed in this paper. J.T. thanks Professors F. Yan and H. Chen for the support of a Chair Professor visiting appointment, during which time this paper was written. We also thank the reviewers for their useful criticisms and suggestions. We are grateful to the Air Force Office of Scientific Research for support through grant award FA9550-08-1-0431 and to the National Science Foundation for instrumental support through grant awards CHE-0443444 and DMR-0414803.

REFERENCES AND NOTES

1. Lin, S. C.; Shih, C. J.; Strano, M. S.; Blankschtein, D. Molecular Insights into the Surface Morphology, Layering Structure, and Aggregation Kinetics of Surfactant-Stabilized Graphene Dispersions. *J. Am. Chem. Soc.* **2011**, *133*, 12810–12823.
2. Shih, C.-J.; Lin, S.; Strano, M. S.; Blankschtein, D. Understanding the Stabilization of Liquid-Phase-Exfoliated Graphene in Polar Solvents: Molecular Dynamics Simulations and Kinetic Theory of Colloid Aggregation. *J. Am. Chem. Soc.* **2010**, *132*, 14638–14648.
3. Seo, J. W. T.; Green, A. A.; Antaris, A. L.; Hersam, M. C. High-Concentration Aqueous Dispersions of Graphene Using Nonionic, Biocompatible Block Copolymers. *J. Phys. Chem. Lett.* **2011**, *2*, 1004–1008.
4. Edwards, R. S.; Coleman, K. S. Graphene Synthesis: Relationship to Applications. *Nanoscale* **2013**, *5*, 38–51.
5. Liang, L. J.; Wu, T.; Kang, Y.; Wang, Q. Dispersion of Graphene Sheets in Aqueous Solution by Oligodeoxynucleotides. *ChemPhysChem* **2013**, *14*, 1626–1632.
6. Sun, D. M.; Liu, C.; Ren, W. C.; Cheng, H. M. A Review of Carbon Nanotube- and Graphene-Based Flexible Thin-Film Transistors. *Small* **2013**, *9*, 1188–1205.
7. Schinwald, A.; Murphy, F. A.; Jones, A.; MacNee, W.; Donaldson, K. Graphene-based nanoplatelets: A New Risk to the Respiratory System As a Consequence of Their Unusual Aerodynamic Properties. *ACS Nano* **2012**, *6*, 736–748.
8. Ma-Hock, L.; Strauss, V.; Treumann, S.; Kutler, K.; Wohlleben, W.; Hofmann, T.; Gröters, S.; Wiench, K.; van Ravenzwaay, B.; Landsiedel, R. Comparative Inhalation Toxicity of Multi-Wall Carbon Nanotubes, Graphene, Graphite Nanoplatelets and Low Surface Carbon Black. *Particle Fibre Toxicol* **2013**, *10*, 23-1.
9. Horvath, L.; Magrez, A.; Burghard, M.; Kern, K.; Ferro, L.; Schwaller, B. Evaluation of the Toxicity of Graphene Derivatives on Cells of the Lung Luminal Surface. *Carbon* **2013**, *64*, 45–60.
10. Wei, D. C.; Wu, B.; Guo, Y. L.; Yu, G.; Liu, Y. N. Controllable Chemical Vapor Deposition Growth of Few Layer Graphene for Electronic Devices. *Acc. Chem. Res.* **2013**, *46*, 106–115.
11. De, S.; Coleman, J. N. Are There Fundamental Limitations on the Sheet Resistance and Transmittance of Thin Graphene Films? *ACS Nano* **2010**, *4*, 2713–2720.
12. Secor, E. B.; Prabhumiarashi, P.; Puntambekar, K.; Geirer, M. L.; Hersam, M. C. Inkjet Printing of High Conductivity, Flexible Graphene Patterns. *J. Phys. Chem. Lett.* **2013**, *4*, 1347–1351.
13. Benwadih, M.; Aliane, A.; Jacob, S.; Bablet, J.; Coppard, R.; Chartier, I. Integration of a Graphene Ink As Gate Electrode for Printed Organic Complementary Thin-Film Transistors. *Org. Electron.* **2014**, *15*, 614–621.
14. Baker, J.; Deganello, D.; Gethin, D. t.; Watson, T. M. Flexographic Printing of Graphene Nanoplatelet Ink to Replace Platinum As Counter Electrode Catalyst in Flexible Dye Sensitised Solar Cell. *Mater. Res. Innovations* **2014**, *18*, 86–90.
15. Janas, D.; Koziol, K. K. A Review of Production Methods of Carbon Nanotube and Graphene Thin Films for Electrochemical Applications. *Nanoscale* **2014**, *6*, 3037–3045.
16. Abbas, A.; Zhao, Y.; Zhou, J. G.; Wang, X. G.; Lin, T. Improving Thermal Conductivity of Cotton Fabrics Using Composite Coatings Containing Graphene, Multiwall Carbon Nanotube or Boron Nitride Fine Particles. *Fibers Polymers* **2013**, *14*, 1641–1649.
17. Xiang, J. L.; Drzal, L. T. Thermal Conductivity of Exfoliated Graphite Nanoplatelet Paper. *Carbon* **2011**, *49*, 773–778.
18. Potts, J. R.; Dreyer, D. R.; Bielawski, C. W.; Ruoff, R. S. Graphene-Based Polymer Nanocomposites. *Polymer* **2011**, *1*, 5–25.
19. Ansari, S.; Giannelis, E. P. Functionalized Graphene Sheet-Poly(Vinylidene Fluoride) Conductive Nanocomposites. *J. Polym. Sci., Part B: Polym. Phys.* **2009**, *9*, 888–897.

20. Xu, Y.; Hong, W.; Bai, H.; Li, C.; Shi, G. Strong and Ductile Poly(Vinyl Alcohol)/Graphene Oxide Composite Films with a Layered Structure. *Carbon* **2009**, *15*, 3538–3543.
21. Martin-Gallego, M.; Verdejo, R.; Lopez-Manchado, M. A.; Sangermano, M. Epoxy-Graphene UV-Cured Nanocomposites. *Polymer* **2011**, *52*, 4664–4669.
22. Kim, G. H.; Hwang, D. H.; Woo, S. I. Thermoelectric Properties of Nanocomposite Thin Films Prepared with Poly(3,4-Ethylenedioxythiophene) Poly(Styrenesulfonate) and Graphene. *Phys. Chem. Chem. Phys.* **2012**, *14*, 3530–3536.
23. Tang, H. X.; Ehlert, G. J.; Lin, Y. R.; Sodano, H. A. Highly Efficient Synthesis of Graphene Nanocomposites. *Nano Lett.* **2012**, *12*, 84–90.
24. Wang, W. J.; Hao, Q. Y.; Lei, W.; Xia, X. F.; Wang, X. Graphene/SnO_2/Polypyrrole Ternary Nanocomposites As Supercapacitor Electrode Materials. *RSC Adv.* **2012**, *2*, 10268–10274.
25. Tjong, S. C. Polymer Composites with Graphene Nanofillers: Electrical Properties and Applications. *J. Nanosci. Nanotech* **2014**, *14*, 1154–1168.
26. Dao, T. D.; Lee, H. I.; Jeong, H. M. Alumina-Coated Graphene Nanosheet and Its Composite of Acrylic Rubber. *J. Colloid Interface Sci.* **2014**, *416*, 38–43.
27. Vasileiou, A. A.; Kontopoulou, M.; Docoslis, A. A noncovalent Compatibilization Approach to Improve the Filler Dispersion and Properties of Polyethylene/Graphene Composites. *ACS Appl. Mater. Interfaces* **2014**, *6*, 1916–1925.
28. Niu, J. J.; Gao, H.; Tian, W. F. Synthesis and Applications of Graphene-Quantum Dot Composites. *Prog. Chem.* **2014**, *26*, 270–276.
29. Avouris, P.; Chen, Z. H.; Perebeinos, V. Carbon-Based Electronics. *Nat. Nanotechnol.* **2007**, *2*, 605–615.
30. Rao, C. N. R.; Sood, A. K.; Subrahmanyam, K. S.; Govindaraj, A. Graphene: The New Two-Dimensional Nanomaterial. *Angew. Chem., Int. Ed.* **2009**, *48*, 7752–7777.
31. Cole, M. W.; Crespi, V. H.; Dresselhaus, M. S.; Dresselhaus, G.; Fischer, J. E.; Gutierrez, H. R.; Kojima, K.; Mahan, G. D.; Rao, A. M.; Sofo, J. O.; et al. Structural, Electronic, Optical and Vibrational Properties of Nanoscale Carbons and Nanowires: A Colloquial Review. *J. Phys.: Condens. Matter* **2010**, *22*, 334201 (25pp).
32. Abergel, D. S. L.; Apalkov, V.; Berashevich, J.; Ziegler, K.; Chakraborty, T. Properties of Graphene: A Theoretical Perspective. *Adv. Phys.* **2010**, *59*, 261–482.
33. Balandin, A. A.; Alexander, A. Thermal Properties of Graphene and Nanostructured Carbon Materials. *Nat. Mater.* **2011**, *10*, 569–581.
34. Tomonari, Y.; Murakami, H.; Nakashima, N. Solubilization of Single-Walled Carbon Nanotubes by Using Polycyclic Aromatic Ammonium Amphiphiles in Water - Strategy for the Design of High-Performance Solubilizers. *Chem.—Eur. J.* **2006**, *12*, 4027–4034.
35. Nepal, D.; Geckler, K. E. pH-Sensitive Dispersion and Debundling of Single-Walled Carbon Nanotubes: Lysozyme As a Tool. *Small* **2006**, *2*, 406–412.
36. Wang, D.; Chen, L. Temperature and pH-Responsive Single-Walled Carbon Nanotube Dispersions. *Nano Lett.* **2007**, *7*, 1480–1484.
37. Rastogi, R.; Kaushal, R.; Tripathi, S. K.; Sharma, A. l.; Kaur, I.; Bharadwaj, L. M. Comparative Study of Carbon Nanotube Dispersion Using Surfactants. *J. Colloid Interface Sci.* **2008**, *328*, 421–428.
38. Sun, Z.; Nicolosi, V.; Rickard, D.; Bergin, S. D.; Aherne, D.; Coleman, J. N. Quantitative Evaluation of Surfactant-Stabilized Single-Walled Carbon Nanotubes: Dispersion Quality and Its Correlation with Zeta Potential. *J. Phys. Chem. C* **2008**, *112*, 10692–10699.
39. Xin, X.; Xu, G.; Zhao, T.; Zhu, Y.; Shi, X.; Gong, H.; Zhang, Z. Dispersing Carbon Nanotubes in Aqueous Solutions by a Starlike Block Copolymer. *J. Phys. Chem. C* **2008**, *112*, 16377–16384.
40. Wang, H. Dispersing Carbon Nanotubes Using Surfactants. *Curr. Opin. Colloid Interface Sci.* **2009**, *14*, 364–371.
41. Vaisman, L.; Marom, G.; Wagner, H. D. Dispersions of Surface-Modified Carbon Nanotubes in Water-Soluble and Water-Insoluble Polymers. *Adv. Funct. Mater.* **2006**, *16*, 357–363.
42. Yu, J. R.; Grossiord, N.; Koning, C. E.; Loos, J. Controlling the Dispersion of Multi-Wall Carbon Nanotubes in Aqueous Surfactant Solution. *Carbon* **2007**, *45*, 618–623.
43. Azoubel, S.; Magdassi, S. The Formation of Carbon Nanotube Dispersions by High Pressure Homogenization and Their Rapid Characterization by Analytical Centrifuge. *Carbon* **2010**, *48*, 3346–3352.
44. Lu, F.; Zhang, S. H.; Zheng, L. Q. Dispersion of Multiwalled Carbon Nanotubes (MWCNTs) by Ionic Liquid-Based Gemini Pyrrolidinium Surfactants in Aqueous Solution. *Colloid Polym. Sci.* **2011**, *289*, 1815–1819.
45. Lu, F.; Zhang, S. H.; Zheng, L. Q. Dispersion of Multi-Walled Carbon Nanotubes (MWCNTs) by Ionic Liquid-Based Phosphonium Surfactants in Aqueous Solution. *J. Mol. Liq.* **2012**, *173*, 42–46.
46. Lützen, H.; Wirts-Rutters, M.; Hartwig, A. Structural Studies of Aromatic Surfactants for Dispergation of Multiwall Carbon Nanotubes. *Soft Mater.* **2012**, *10*, 462–471.
47. Bai, Y. C.; Wu, F. C.; Lin, D. H.; Xing, B. S. Aqueous Stabilization of Carbon Nanotubes: Effects of Surface Oxidization and Solution Chemistry. *Env. Sci. Pollution Res.* **2014**, *21*, 4358–4365.
48. Blake, P.; Brimicombe, P. D.; Nair, R. R.; Booth, T. J.; Jiang, D.; Schedin, F.; Ponomarenko, L. A.; Morozov, S. V.; Gleeson, H. F.; Hill, E. W.; et al. Graphene-Based Liquid Crystal Device. *Nano Lett.* **2008**, *8*, 1704–1708.
49. Hernandez, Y.; Nicolosi, V.; Lotya, M.; Blighe, F. M.; Sun, Z.; De, S.; McGovern, I. T.; Holland, B.; Byrne, M.; Gun'Ko, Y. K.; et al. High-Yield Production of Graphene by Liquid-Phase Exfoliation of Graphite. *Nat. Nanotechnol.* **2008**, *3*, 563–568.
50. Behabtu, N.; Lomeda, J. R.; Green, M. J.; Higginbotham, A. L.; Sinitskii, A.; Kosynkin, D. V.; Tsentalovich, D.; Parra-Vasquez, A.; Schmidt, J.; Kesselman, E.; et al. Spontaneous High-Concentration Dispersions and Liquid Crystals of Graphene. *Nat. Nanotechnol.* **2010**, *6*, 406–411.
51. Khan, U.; O'Neil, A.; Loyta, M.; De, S.; Coleman, J. N. High Concentration Solvent Exfoliation of Graphene. *Small* **2010**, *6*, 864–871.
52. Park, K. H.; Kim, B. H.; Song, S. H.; Kwon, J. Y.; Kong, B. S.; Kang, K. S.; Jeon, S. W. Exfoliation of Non-Oxidized Graphene Flakes for Scalable Conductive Film. *Nano Lett.* **2012**, *12*, 2871–2876.
53. Quintana, M.; Vazquez, E.; Prato, M. Organic Functionalization of Graphene in Dispersions. *Acc. Chem. Res.* **2013**, *46*, 138–148.
54. Zhu, L.; Zhao, X.; Li, Y.; Yu, X.; Li, C.; Zhang, Q. High-Quality Production of Graphene by Liquid-Phase Exfoliation of Expanded Graphite. *Mater. Chem. Phys.* **2013**, *137*, 984–990.
55. Coleman, J. N. Liquid Exfoliation of Defect-Free Graphene. *Acc. Chem. Res.* **2013**, *46*, 14–22.
56. Stankovich, S.; Dikin, D. A.; Piner, R. D.; Kohlhaas, K. A.; Kleinhammes, A.; Jia, Y.; Wu, Y.; Nguyen, S. T.; Ruoff, R. S. Stable Aqueous Dispersions of Graphitic Nanoplatelets *via* the Reduction of Exfoliated Graphite Oxide in the Presence of Poly(Sodium 4-Styrenesulfonate). *Carbon* **2007**, *45*, 1558–1565.
57. Kang, S. M.; Park, S.; Kim, D.; Park, S. Y.; Ruoff, R. S.; Lee, H. Simultaneous Reduction and Surface Functionalization of Graphene Oxide by Mussel-Inspired Chemistry. *Adv. Funct. Mater.* **2011**, *21*, 108–112.
58. Malig, J.; Jux, N.; Guldi, D. M. Toward Multifunctional Wet Chemically Functionalized Graphene – Integration of Oligomeric, Molecular, and Particulate Building Blocks That Reveal Photoactivity and Redox Activity. *Acc. Chem. Res.* **2013**, *46*, 53–64.
59. Hsieh, A. G.; Korkut, S.; Punckt, C.; Aksay, I. A. Dispersion Stability of Functionalized Graphene in Aqueous Sodium Dodecyl Sulfate Solutions. *Langmuir* **2013**, *29*, 14831–14838.

60. Paulus, G. L. C.; Wang, Q. H.; Strano, M. S. Covalent Electron Transfer Chemistry of Graphene with Diazonium Salts. *Acc. Chem. Res.* **2013**, *46*, 160–170.
61. Kelly, K. F.; Billups, W. W. Synthesis of Soluble Graphite and Graphene. *Acc. Chem. Res.* **2013**, *46*, 4–13.
62. Muller, T.; Xia, F.; Avouris, P. Graphene Photodetectors for High-Speed Optical Communications. *Nat. Photonics* **2010**, *4*, 297–301.
63. Herman, L. H.; Kim, C.-J.; Wang, Z. H.; Jo, M.-H.; Park, J. W. Depolarization Effect in Optical Absorption Measurements of One- and Two-Dimensional Nanostructures. *Appl. Phys. Lett.* **2012**, *101*, 123102 (4 pp).
64. Lotya, M.; King, P. J.; Khan, U.; De, S.; Coleman, J. N. High-Concentration, Surfactant-Stabilized Graphene Dispersions. *ACS Nano* **2010**, *4*, 3155–3162.
65. Nuvoli, D.; Valentini, L.; Alzari, V.; Scognamillo, S.; Bon, S. B.; Piccinini, M.; Illescas, J.; Mariani, A. High Concentration Few-Layer Graphene Sheets Obtained by Liquid Phase Exfoliation of Graphite in Ionic Liquid. *J. Mater. Chem.* **2011**, *21*, 3428–3431.
66. Ghislandi, M.; Tkalya, E.; Schillinger, S.; Koning, C. E.; de With, G. High Performance Graphene- and MWCNTs-Based PS/PPO Composites Obtained *via* Organic Solvent Dispersion. *Compos. Sci. Technol.* **2013**, *80*, 16–22.
67. Barwich, S.; Khan, U.; Coleman, J. N. A Technique to Pretreat Graphite Which Allows the Rapid Dispersion of Defect-Free Graphene in Solvents at High Concentration. *J. Phys. Chem. C* **2013**, *117*, 19212–19218.
68. Gayathri, S.; Jayabal, P.; Kottaisam, M.; Ramakrishnan, V. Synthesis of Few Layer Graphene by Direct Exfoliation of Graphite and a Raman Spectroscopic Study. *AIP Advances* **2014**, *4*, 027116 (12 pp).
69. Jeong, S. H.; Kim, K. K.; Jeong, S. J.; Ann, K. H.; Lee, S. H.; Lee, Y. H. Optical Absorption Spectroscopy for Determining Carbon Nanotube Concentration in Solution. *Synth. Met.* **2007**, *157*, 570–574.
70. Grossiord, N. Thesis. *A Latex-Based Concept for Making Carbon Nanotube/Polymer Nanocomposites*, Technische Universiteit Eindhoven, 2007, http://alexandria.tue.nl/extra_2/200712265.pdf, downloaded 25 May 2012.
71. Krause, B.; Petzold, G.; Pegel, S.; Pötschke, P. Correlation of Carbon Nanotube Dispersability in Aqueous Surfactant Solutions and Polymers. *Carbon* **2009**, *47*, 602–612.
72. Antonietti, M.; Shen, Y.; Nakanishi, T.; Manuelian, M.; Campbell, R.; Gwee, L.; Elabd, Y.; Tambe, N.; Crombez, R.; Texter, J. Single-Wall Carbon Nanotube Latexes. *ACS Appl. Mater. Interfaces* **2010**, *2*, 649–653.
73. Lu, J.; Yan, F.; Texter, J. Advanced Applications of Ionic Liquids in Polymer Science. *Prog. Polym. Sci.* **2009**, *34*, 431–448.
74. Green, M. D.; Long, T. E. Designing Imidazole-Based Ionic Liquids and Ionic Liquid Monomers for Emerging Technologies. *Polym. Rev.* **2009**, *49*, 291–314.
75. Mecerreyes, D. Polymeric Ionic Liquids: Broadening the Properties and Applications of Polyelectrolytes. *Prog. Polym. Sci.* **2011**, *36*, 1629–1648.
76. Yuan, J. Y.; Antonietti, M. Poly(Ionic Liquid)s: Polymers Expanding Classical Property Profiles. *Polymer* **2011**, *52*, 1469–1482.
77. Yuan, J. Y.; Mecerreyes, D.; Antonietti, M. Poly(Ionic Liquid)s: An Update. *Prog. Polym. Sci.* **2013**, *38*, 1009–1036.
78. Yan, F.; Texter, J. Surfactant Ionic Liquid-Based Microemulsions for Polymerization. *Chem. Commun.* **2006**, *42*, 2696–2698.
79. Yan, F.; Texter, J. Solvent-Reversible Poration in Ionic Liquid Copolymers. *Angew. Chem., Int. Ed.* **2007**, *46*, 2440–2443.
80. Texter, J. Anion Responsive Imidazolium-Based Polymers. *Macromol. Rap. Commun.* **2012**, *33*, 1996–2014.
81. Texter, J. Ionic Liquids and Polymeric Ionic Liquids as Stimuli Responsive Functional Materials. in *Handbook of Ionic Liquids*; Mecerreyes, D., Ed., Springer: Darmstadt, 2014; in press.
82. Zhao, L.; Crombez, R.; Antonietti, M.; Texter, J.; Titirici, M.-M. Sustainable Nitrogen-Doped Carbon Latexes with High Electrical and Thermal Conductivity;. *Polymer* **2010**, *51*, 4540–4546.
83. Giordano, C.; Yang, W.; Lindemann, A.; Crombez, R.; Texter, J. Waterborne WC Nanodispersions. *Colloids Surfaces A* **2011**, *374*, 84–87.
84. Texter, J. Nanoparticle Dispersions with Ionic Liquid-Based Stabilizers. US Patent Application Publication, US 2011/0233458 A1, 29 Sep 2011.
85. Texter, J.; Ager, D. Waterborne Graphene Dispersions and Advanced Coatings. *Prepr. Symp.-Am. Chem. Soc., Div. Fuel Chem.* **2012**, *57*, 90–92.
86. Texter, J.; Ager, D.; Arjunan Vasantha, V.; Crombez, R.; England, D.; Ma, X.; Maniglia, R.; Tambe, N. Advanced Nanocarbon Materials Facilitated by Novel Stimuli-Responsive Stabilizers. *Chem. Lett.* **2012**, *41*, 1377–1379.
87. Texter, J.; Arjunan Vasantha, V.; Maniglia, R.; Slater, L.; Mourey, T. Triblock Copolymer Based on Poly(Propylene Oxide) and Poly(1-[11-Acryloyloxyundecyl]-3-Methyl-Imidazolium Bromide**)**. *Macromol. Rap. Commun.* **2012**, *33*, 69–74.
88. England, D.; Yan, F.; Texter, J. Porating Anion-Responsive Copolymeric Gels. *Langmuir* **2013**, *29*, 12013–12024.
89. England, D.; Tambe, N.; Texter, J. Stimuli-Responsive Nanolatexes – Porating Films. *ACS Macro Lett.* **2012**, *1*, 310–314.
90. Buzaglo, M.; Shtein, M.; Kober, S.; Lovrincic, R.; Vilan, A.; Regev, O. Critical Parameters in Exfoliating Graphite into Graphene. *Phys. Chem. Chem. Phys.* **2013**, *15*, 4428–4435.
91. Green, A. A.; Hersam, M. C. Solution Phase Production of Graphene with Controlled Thickness *via* Density Differentiation. *Nano Lett.* **2009**, *9*, 4031–4036.
92. Lu, Z.; Robinson, J. T.; Sun, X. M.; Dai, H. J. PEGylated Nanographene Oxide for Delivery of Water-Insoluble Cancer Drugs. *J. Am. Chem. Soc.* **2008**, *130*, 10876–10877.
93. Li, D.; Mueller, M. B.; Gilje, S.; Kaner, R. B.; Wallace, G. G. Processable Aqueous Dispersions of Graphene Nanosheets. *Nat. Nanotechnol.* **2008**, *3*, 101–105.
94. Mehta, A.; Nelson, E. J.; Webb, S. M.; Jolt, J. K. The Interaction of Bromide Ions with Graphitic Materials. *Adv. Mater.* **2009**, *21*, 102–106.
95. Watanabe, T.; Okabayashi, M.; Kurokawa, D.; Nishimoto, Y.; Ozawa, T.; Kawasakia, H.; Arakawa, R. Determination of Primary Bond Scissions by Mass Spectrometric Analysis of Ultrasonic Degradation Products of Poly(Ethylene Oxide-*Block*-Propylene Oxide) Copolymers. *J. Mass. Spectrom.* **2010**, *45*, 799–805.
96. Akyüz, A.; Catalgil-Giz, H.; Giz, A. T. Kinetics of Ultrasonic Polymer Degradation: Comparison of Theoretical Models with On-Line Data. *Macromol. Chem. Phys.* **2008**, *209*, 801–809.
97. Arakawa, R.; Kawasaki, H. Mass Spectrometric Analysis of Synthetic Polymers Using Ultrasonic Degradation. *Bunseki Kagaru* **2011**, *60*, 198–214.
98. Vinu, R. Madras, G. Kinetics of Sono-Photooxidative Degradation of Poly(Alkyl Methacrylate)s. *Ultrasonics Sonochem.* **2011**, *18*, 608–616.
99. Shukla, B. S.; Darabonia, N.; Madras, G. Ultrasonic Degradation of Poly(Acrylic Acid). *J. Appl. Polym. Sci.* **2009**, *112*, 991–997.
100. Nair, R. R.; Blake, P.; Grigorenko, A. N.; Novoselov, K. S.; Booth, T. J.; Stauber, T.; Peres, N. M. R.; Geim, A. K. Fine Structure Constant Defines Visual Transparency of Graphene. *Science* **2008**, *320*, 1308–1308.
101. Geim, A. K.; Novoselov, K. S. The structure of Suspended Graphene Sheets. *Nat. Mater.* **2007**, *446*, 183–191.
102. Mak, K. F.; Sfeir, M. Y.; Wu, Y.; Lui, C. H.; Misewich, J. A.; Heinz, T. F. Measurement of the Optical Conductivity of Graphene. *Phys. Rev. Lett.* **2008**, *101*, 196405 (4 pp).
103. Herman, L. H.; Kim, C.-J.; Wang, Z.; Jo, M.-H.; Park, J. Depolarization Effect in Optical Absorption Measurements of One- and Two-Dimensional Nanostructures. *Appl. Phys. Lett.* **2012**, *101*, 123101 (4 pp).
104. Mak, K. F.; Shan, J.; Heinz, T. F. Seeing Many-Body Effects in Single- and Few-Layer Graphene: Observation of Two-Dimensional Saddle-Point Excitons. *Phys. Rev. Lett.* **2011**, *106*, 046401 (4 pp).

105. He, Y.; Chen, W. F.; Yu, W. B.; Ouyang, G.; Yang, G. W. Anomalous Interface Adhesion of Graphene Membranes. *Sci. Rep* **2013**, *3*, 2660 (7 pp).
106. Varchon, F.; Feng, R.; Hass, J.; Li, X.; Nguyen, B. N.; Naud, C.; Mallet, P.; Veuillen, J.-Y.; Berger, C.; Conrad, E. H.; *et al.* Electronic Structure of Epitaxial Graphene Layers on SiC: Effect of the Substrate. *Phys. Rev. Lett.* **2007**, *99*, 126805.
107. Weber, J. W.; Calado, V. E.; van de Sanden, M. C. M. Optical Constants of Graphene Measured by Spectroscopic Ellipsometry. *Appl. Phys. Lett.* **2010**, *97*, 091904.
108. Kim, S. Y.; Park, H. S. On the Effective Plate Thickness of Monolayer Graphene from Flexural Wave Propagation. *J. Appl. Phys.* **201**, *110*, 054324.
109. Wang, W. E.; Balooch, M.; Claypool, C.; Zawaideh, M.; Farnaam, K. Combined Reflectometry-Ellipsometry Technique to Measure Graphite Down to Monolayer Thickness. *Solid State Technol.* **2009**, *52*, 18–21.
110. Gray, A.; Balooch, M.; Allegret, S.; De Gendt, S.; Wang, W.-E. Optical Detection and Characterization of Graphene by Broadband Spectrophotometry. *J. Appl. Phys.* **2008**, *104*, 053109.
111. Saito, R.; Kataura, H. Optical Properties, Ch. 9, In *Carbon Nanotubes*, Dresselhaus, M. S.; Dresselhaus, G.; Avouris, P., Editors, *Topics Appl. Phys.* **2001**, *80*, 216−250.
112. Kamal, J. S.; Gomes, R.; Hens, Z.; Karvar, M.; Neyts, K.; Compernolle, S.; Vanhaecke, F. Direct Determination of Absorption Anisotropy in Colloidal Quantum Rods. *Phys. Rev. B* **2012**, *85*, 035126. The parallel and perpendicular directions for the absorption coefficients were applied to the quantum rod axisymmetric axis and transverse directions, respectively, and refer to the applied electric field polarizations. These definitions are expressed explicitly in the supporting information for this reference. For the purposes of this paper, a graphene sheet is placed centered at the origin perpendicular to this quantum rod. Directions parallel to this graphene sheet correspond to the perpendicular polarization of this reference, and the graphene normal corresponds to the rod axisymmetric axis, the parallel polarization of this reference.
113. Johnson, L. G.; Dresselhaus, G. Optical Properties of Graphite. *Phys. Rev. B* **1973**, *7*, 2275–2285.
114. Bruna, M.; Borini, S. Optical Constants of Graphene Layers in the Visible Range. *Appl. Phys. Lett.* **2009**, *94*, 031901.
115. Teller, E. Crossing of Potential Surfaces. *J. Phys. Chem.* **1937**, *41*, 109–116.
116. Jahn, H. A.; Teller, E. Stability of Polyatomic Molecules in Degenerate Electronic States 1. Orbital Degeneracy. *Proc. R. Soc. A* **1937**, *161*, 220–235.
117. Englman, R. *The Jahn-Teller Effect in Molecules and Crystals*; Wiley, London,(1972).
118. Metlov, K. L. Model for Flexural Phonon Dispersion in Graphite and Graphene. *Phys. Rev. B* **2010**, *82*, 033404.
119. Castro Neto, A. H.; Guinea, F.; Peres, N. M. R.; Novoselov, K. S.; Geim, A. K. The Electronic Properties of Graphene. *Rev. Mod. Phys.* **2009**, *81*, 109–162.
120. Yang, L.; Deslippe, J.; Park, C.-H.; Cohen, M. L.; Louie, S. G. Excitonic Effects on the Optical Response of Graphene and Bilayer Graphene. *Phys. Rev. Lett.* **2009**, *103*, 186802.
121. Kravets, V. G.; Grigorenko, A. N.; Hair, R. R.; Blake, P.; Anissimova, S.; Novoselov, K. S.; Geim, A. K. Spectroscopic Ellipsometry of Graphene and an Exciton-Shifted Van Hove Peak in Absorption. *Phys. Rev. B* **2010**, *81*, 155413 (6 pp).
122. Matkovic, A.; Beltaos, A.; Milicevic, M.; Ralevic, U.; Vasic, B.; Jovanovic, D.; Gajic, R. Spectroscopic Imaging Ellipsometry and Fano Resonance Modeling of Graphene. *J. Appl. Phys.* **2012**, *112*, 123523.
123. Chae, D.-H.; Utikal, T.; Weisenburger, S.; Giessen, H.; von, K.; itzing, K.; Lippitz, M.; Smet, J. Excitonic Fano Resonance in Free-Standing Graphene. *Nano Lett.* **2011**, *11*, 1379–1382.
124. Lotya, M.; Hernandez, Y.; King, P. J.; Smith, R. J.; Nicolosi, V.; Karlsson, L. S.; Blighe, F. N.; De, S.; Wang, Z.; McGovern, I. T.; *et al.* Liquid Phase Production of Graphene by Exfoliation of Graphite in Surfactant/Water Solutions. *J. Am. Chem. Soc.* **2009**, *131*, 3611–3620.
125. Nuvoli, D.; Alzari, V.; Sanna, R.; Scognamillo, S.; Piccinini, M.; Peponi, L.; Kenny, J. M.; Mariani, A. The Production of Concentrated Dispersions of Few-Layer Graphene by the Direct Exfoliation of Graphite in Organosilanes. *Nanoscale Res. Lett.* **2012**, *7*, 674.
126. Decher, G. Fuzzy Nanoassemblies: Toward Layered Polymeric Multicomposites. *Science* **1997**, *277*, 1232–1237.
127. Shen, J. F.; Hu, Y. Z.; Li, C.; Qin, C.; Shi, M.; Ye, M. X. Layer-by-Layer Self-Assembly of Graphene Nanoplatelets. *Langmuir* **2009**, *25*, 6122–6128.
128. Zhang, J.; Zou, H. L.; Qing, Q.; Yang, Y. L.; Li, Q. W.; Liu, Z. F.; Guo, X. Y.; Du, Z. L. Effect of Chemical Oxidation on the Structure of Single-Walled Carbon Nanotubes. *J. Phys. Chem. B* **2003**, *107*, 3712–3718.
129. Taft, E. A.; Philipp, H. R. Optical Properties of Graphite. *Phys. Rev.* **1965**, *138*, A197–A202.
130. Preil, M. E.; Tatar, R. C.; Di Vincenzo, D. P.; Fischer, J. E. Dielectric Function and Critical-Point Transitions in Boron-Doped Graphite. *Phys. Rev. B* **1982**, *26*, 4674–4679.
131. Li, Z. Q.; Tsai, S.-W.; Padilla, W. J.; Dordevic, S. V.; Burch, K. S.; Wang, Y. J.; Basov, D. N. Infrared Probe of the Anomalous Magnetotransport of Highly Oriented Pyrolytic Graphite in the Extreme Quantum Limit. *Phys. Rev. B* **2006**, *74*, 195404.
132. Brown, A. B. D.; Rennie, A. R. Images of Shear-Induced Phase Separation in a Dispersion of Hard Nanoscale Discs. *Chem. Eng. Sci.* **2001**, *56*, 2999–3004.
133. Melosh, N. A.; Davidson, P.; Feng, P.; Pine, D. J.; Chmelka, B. F. Macroscopic Shear Alignment of Bulk Transparent Mesostructured Silica. *J. Am. Chem. Soc.* **2001**, *123*, 1240–1241.
134. Yoonessi, M.; Toghiani, H.; Pittman, C. U., Jr. Orientation of Montmorillonite Clay in Dicyclopentadiene/Organically Modified Clay Dispersions and Nanocomposites. *J. Appl. Polym. Sci.* **2006**, *102*, 2743–2751.
135. Fartaria, R. P. S.; Javid, N.; Sefcik, J.; Sweatman, M. B. Simulation of Scattering and Phase Behavior Around the Isotropic−Nematic Transition of Discotic Particles. *J. Colloid Interface Sci.* **2012**, *377*, 94–104.
136. Guu, D.; Dhont, J. K. G.; Lettinga, M. P. Dispersions and Mixtures of Particles with Complex Architectures in Shear Flow. *Eur. Phys. J. Special Topics* **2013**, *222*, 2739–2755.
137. Chen, H. Q.; Müller, M. B.; Gilmore, K. J.; Wallace, G. G.; Li, D. Mechanically Strong, Electrically Conductive, and Biocompatible Graphene Paper. *Adv. Mater.* **2008**, *20*, 3557–3561.
138. Wu, H.; Drzal, L. T. Graphene Nanoplatelet Paper As a Light-Weight Composite with Excellent Electrical and Thermal Conductivity and Good Gas Barrier Properties. *Carbon* **2012**, *50*, 1135–1145.
139. Marcilla, R.; Curri, M. L.; Cozzoli, P. D.; Martínez, M. T.; Loinaz, I.; Grande, H.; Pomposo, J. A.; Mecerreyes, D. Nano-Objects on a Round Trip from Water to Organics in a Polymeric Ionic Liquid Vehicle. *Small* **2006**, *2*, 507–512.
140. Kim, T. Y.; Lee, H. W.; Kim, J. E.; Suh, K. S. Synthesis of Phase Transferable Graphene Sheets Using Ionic Liquid Polymers. *ACS Nano* **2010**, *4*, 1612–1618.
141. Men, Y. J.; Li, X.-H.; Antonietti, M.; Yuan, J. Poly(Tetrabutylphosphonium 4-Styrenesulfonate): a Poly(Ionic Liquid) Stabilizer for Graphene Being Multi-Responsive. *Polym. Chem.* **2012**, *3*, 871–874.
142. Texter, J. Graphene Dispersions. *Curr. Opinion Colloid Surface Sci.* **2014**, *19*, 163–174.